Article

# Polymorphism of Zn[Au(CN)] and Its Luminescent Sensory Response to NH Vapor

Michael J. Katz, Taramatee Ramnial, Hua-Zhong Yu, and Daniel B. Leznoff

*J. Am. Chem. Soc.*, **2008**, 130 (32), 10662-10673 • DOI: 10.1021/ja801773p • Publication Date (Web): 19 July 2008



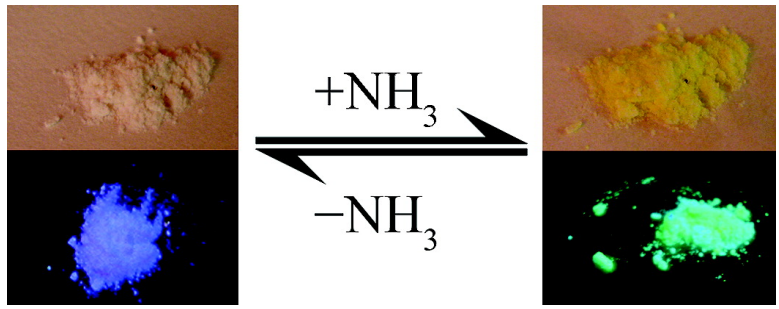

J|A|C|S
ARTICLES

Published on Web 07/19/2008

# Polymorphism of $Zn[Au(CN)_2]_2$ and Its Luminescent Sensory Response to $NH_3$ Vapor

Michael J. Katz, Taramatee Ramnial, Hua-Zhong Yu, and Daniel B. Leznoff*

*Department of Chemistry, Simon Fraser University, 8888 University Drive, Burnaby, British Columbia, Canada V5A 1S6*

Received March 10, 2008; E-mail: dleznoff@sfu.ca

***Abstract:*** Four polymorphic forms of the complex $Zn[Au(CN)_2]_2$ have been synthesized and both structurally and spectroscopically characterized. In each of the four polymorphs, a zinc center in a tetrahedral geometry with a $Au(CN)_2^-$ unit at each tetrahedral vertex is observed. All four structures contain three-dimensional networks based on corner-sharing tetrahedra. Because of the long $Au(CN)_2^-$ bridging unit, the extra space not occupied by one network is filled by two to five additional interpenetrated networks. Short gold−gold bonds with lengths ranging from 3.11 to 3.33 Å hold the interpenetrated networks together. Three of the four polymorphs are luminescent, having solid-state emissions with wavelengths ranging from 390 to 480 nm. A linear correlation between the emission energy and the gold−gold distance was observed. Upon exposure to ammonia vapor, the polymers altered their structures and emission energies, with the emission wavelength shifting to 500 nm for $\{Zn(NH_3)_2[Au(CN)_2]_2\}$, which adopts a two-dimensional layer structure with octahedral, trans-oriented $NH_3$ groups. The adsorption route is dependent on the polymorph used, with $NH_3$ detection limits as low as 1 ppb. Desorption of the ammonia occurred over 30 min at room temperature.

## Introduction

Coordination polymer research strives to design and synthetically assemble metal and ligand building blocks in a controllable fashion so that the resultant polymer structure exhibits a particular targeted property,[1–3] such as magnetism,[4–7] porosity,[8–12] luminescence,[13–15] vapochromism,[16–20] or conductivity.[21,22] A high level of synthetic control has been achieved in a range of systems, notably metal carboxylate-based metal−organic frameworks (MOFs)[12,23–25] and simple bimetallic hexa-[6] and tetracyanometallate coordination polymers such as Prussian Blue-[7,26] and Hoffman-type clathrates.[27] In particular, the straightforward synthesis of the cyanometallate polymers (usually from aqueous or alcohol solution) facilitates the controlled substitution of the metal in either the cation or the anionic hexa- or tetracyanometallate while keeping an isostructural polymer framework. This powerful design feature has been exploited to probe structure−property relationships (e.g., magnetic, host−guest) of these cyanometallate polymers as a function of their constituents.[28,29]

(1) Janiak, C. *Dalton Trans.* **2003**, 2781.
(2) Steel, P. J. *Acc. Chem. Res.* **2005**, *38*, 243.
(3) Decurtins, S.; Pellaux, R.; Antorrena, G.; Palacio, F. *Coord. Chem. Rev.* **1999**, *190−192*, 841.
(4) Kaneko, W.; Kitagawa, S.; Ohba, M. *J. Am. Chem. Soc.* **2007**, *129*, 248.
(5) Batten, S. R.; Murray, K. S. *Coord. Chem. Rev.* **2003**, *246*, 103.
(6) Ohba, M.; Ôkawa, H. *Coord. Chem. Rev.* **2000**, *198*, 313.
(7) Verdaguer, M.; Bleuzen, A.; Marvaud, V.; Vaissermann, J.; Seuleiman, M.; Desplanches, C.; Scuiller, A.; Train, C.; Garde, R.; Gelly, G.; Lomenech, C.; Rosenman, I.; Veillet, P.; Cartier, C.; Villain, F. *Coord. Chem. Rev.* **1999**, *190−192*, 1023.
(8) Kitagawa, S.; Uemura, K. *Chem. Soc. Rev.* **2005**, *34*, 109.
(9) Kesanli, B.; Lin, W. *Coord. Chem. Rev.* **2003**, *246*, 305.
(10) Banerjee, R.; Phan, A.; Wang, B.; Knobler, C.; Furukawa, H.; O'Keeffe, M.; Yaghi, O. M. *Science* **2008**, *319*, 939.
(11) Rudkevich, D. M. *Angew. Chem., Int. Ed.* **2004**, *43*, 558.
(12) Yaghi, O. M.; Li, H.; Davis, C.; Richardson, D.; Groy, T. L. *Acc. Chem. Res.* **1998**, *31*, 474.
(13) Sun, S.-S.; Lees, A. J. *Coord. Chem. Rev.* **2002**, *230*, 170.
(14) Catalano, V. J.; Etogo, A. O. *J. Organomet. Chem.* **2005**, *690*, 6041.
(15) Fernández, E. J.; Laguna, A.; López-de-Luzuriaga, J. M. *Dalton Trans.* **2007**, 1969.
(16) Wadas, T. J.; Wang, Q.-M.; Kim, Y.-J.; Flaschenreim, C.; Blanton, T. N.; Eisenberg, R. *J. Am. Chem. Soc.* **2004**, *126*, 16841.
(17) Lefebvre, J.; Batchelor, R. J.; Leznoff, D. B. *J. Am. Chem. Soc.* **2004**, *126*, 16117.
(18) Drew, S. M.; Janzen, D. E.; Buss, C. E.; MacEwan, D. I.; Dublin, K. M.; Mann, K. R. *J. Am. Chem. Soc.* **2001**, *123*, 8414.
(19) Dylla, A. G.; Janzen, D. E.; Pomije, M. K.; Mann, K. R. *Organometallics* **2007**, *26*, 6243.
(20) Vickery, J. C.; Olmstead, M. M.; Fung, E. Y.; Balch, A. L. *Angew. Chem., Int. Ed.* **1997**, *36*, 1179.
(21) Tadokoro, M.; Yasuzuka, S.; Nakamura, M.; Shinoda, T.; Tatenuma, T.; Mitsumi, M.; Ozawa, Y.; Toriumi, K.; Yoshino, H.; Shiomi, D.; Sato, K.; Takui, T.; Mori, T.; Murata, K. *Angew. Chem., Int. Ed.* **2006**, *45*, 5144.
(22) Turner, D. L.; Vaid, T. P.; Stephens, P. W.; Stone, K. H.; DiPasquale, A. G.; Rheingold, A. L. *J. Am. Chem. Soc.* **2008**, *130*, 14.
(23) Ye, B.-H.; Tong, M.-L.; Chen, X.-M. *Coord. Chem. Rev.* **2005**, *249*, 545.
(24) Bauer, C. A.; Timofeeva, T. V.; Settersten, T. B.; Patterson, B. D.; Liu, V. H.; Simmons, B. A.; Allendorf, M. D. *J. Am. Chem. Soc.* **2007**, *129*, 7136.
(25) Eddaoudi, M.; Moler, D. B.; Li, H.; Chen, B.; Reineke, T. M.; O'Keeffe, M.; Yaghi, O. M. *Acc. Chem. Res.* **2001**, *34*, 319.
(26) Miller, J. S.; Drillon, M. *Magnetism: Molecules to Materials V*; Wiley: New York, 2005.
(27) Iwamoto, T. In *Comprehensive Supramolecular Chemistry*; Lehn, J. M., Atwood, J. L., Davies, J. E. D., MacNicol, D. D., Vögtle, F., Alberti, G., Bein, T., Eds.; Pergamon Press: Oxford, U.K., 1996.
(28) Lefebvre, J.; Leznoff, D. B. In *Metal and Metalloid-Containing Polymers*; Abd-El-Aziz, A. S., Carraher, C. E., Jr., Pittman, C. U., Jr., Zeldin, M., Eds.; Wiley: New York, 2005; Vol. 5, p 155.
(29) Dunbar, K. R.; Heintz, R. A. *Prog. Inorg. Chem.* **1997**, *45*, 283.


**10.1021/ja801773p CCC: $40.75** 

Despite the popularity and importance of cyanometallate coordination polymers, most studies have focused on utilizing the aforementioned octahedral or square-planar cyanometallate building blocks.[6,27,28] In contrast, the linear $d^{10}$ $Au(CN)_2^-$ unit has been relatively neglected, despite the capability of $Au(CN)_2^-$ to increase structural dimensionality and complexity[30–32] as well as thermal stability[33] through the formation of $d^{10}$ gold−gold (aurophilic) interactions.[34–36] Furthermore, both polymeric and molecular complexes containing gold−gold bonds are often luminescent.[37,38] The emission energies of these luminescent compounds are extremely sensitive to the distance between neighboring gold atoms.[39–41] In the absence of gold−gold bonds, no luminescence is observed for linear Au(I) systems.[38]

Indeed, simple bimetallic systems with $Au(CN)_2^-$ have shown interesting magnetic,[42] luminescent,[43–46] and birefringent properties.[47] Along these lines, we reported that the organic-ligand-free $Cu(\mu\text{-}H_2O)_2[Au(CN)_2]_2$ polymer, which forms a rare water-bridged ribbon structure,[42] shows strong vapochromism in both the visible-absorption and $\nu_{CN}$ IR spectral regions.[17] Specifically, the Cu(II)-coordinated aqua ligands are easily substituted when the solid is exposed to a variety of vapors containing donor atoms, with concomitant changes in color, IR spectrum, and crystal structure.[17] Depending on the basicity and size of the vapor donor molecules, the adsorption process can be reversible at room temperature. The ability of these polymers to adsorb and desorb various donors has been attributed to the flexibility of the Cu(II) ion coordination sphere (with observed coordination numbers of 4−6), and stabilization by the flexible cyanoaurate polymer framework.

Although the aforementioned $Cu(\mu\text{-}H_2O)_2[Au(CN)_2]_2$ system can function as an effective vapochromic sensor material, there are potentially complicating issues in certain applications. For example, strong Lewis base donors such as ammonia bind irreversibly at room temperature, thereby limiting the material to be used as a dosimeter or one-time sensor. In addition, water binds competitively with weak donors or at low analyte concentrations. Also, while the use of a color change as a sensory response is excellent for visual sensing/alert purposes,[48] the absolute sensitivity is limited in this case since the various analyte absorption peaks overlap to a certain extent.

In order to address these issues, substitution of $d^9$ Cu(II) with colorless $d^{10}$ Zn(II) was considered, with the knowledge that the $d^{10}$ Zn(II) coordination sphere is also very flexible.[49] Since Zn(II) would remain colorless regardless of the analyte present, the lack of metal-based visible absorption bands could unmask any gold-based emission. It should be noted that no emission has been observed for the $d^9$ Cu(II) system at room temperature. Changing the detection method from absorption to luminescence could potentially increase analyte sensitivity, since emission is an absolute measurement, as opposed to absorption, which is relative. Although the requisite coordination polymer, $Zn[Au(CN)_2]_2$, had been previously reported[50] and contains short gold−gold bonds, no luminescence properties were described. Furthermore, the polymer contains no water molecules in its structure despite being crystallized from water, suggesting that competitive $H_2O$ binding could be reduced. We therefore initiated an examination of the reaction of $Zn[Au(CN)_2]_2$ with $NH_3$ for comparison with the similar Cu(II) system. However, the deceptively simple Zn(II) system showed some remarkable features. Here we report on the synthesis, structure, and photoluminescent properties of *four polymorphs* of $Zn[Au(CN)_2]_2$ that can reversibly bind $NH_3$ with very high sensitivities, as detected via concomitant changes in their emission energies.

## Experimental Section

**General Procedures and Physical Measurements.** All of the manipulations were performed in air. $[(n\text{-}Bu)_4N][Au(CN)_2]\cdot{}^1/_2H_2O$ was synthesized as previously described.[51] All of the other reagents were obtained from commercial sources and used as received. IR spectra of pressed KBr pellets were recorded on a Thermo Nicolet Nexus 670 FT-IR spectrometer. Microanalyses (C, H, N) were performed at Simon Fraser University on a Carlo Erba EA 1110 CHN elemental analyzer. Thermogravimetric analysis (TGA) data were collected using a Shimadzu TGA-50 instrument heating at 1 °C/min in an air atmosphere. Differential scanning calorimetry (DSC) measurements were performed on a PerkinElmer DSC 7 instrument with a PerkinElmer TAC 7/DX controller heating at 2 °C/min from 25 to 300 °C.

Solid-state luminescence data were collected at room temperature on a Photon Technology International fluorometer using a Xe arc lamp and a photomultiplier detector. Finely ground powder samples were drop-cast from the synthesis solvent onto a quartz plate and placed at a 45° angle in a quartz cuvette. Ammonia exposure experiments were conducted under the same conditions, with the top of the cuvette sealed with parafilm to prevent rapid loss of ammonia gas. The headspace of a bottle of concentrated (29.4%) ammonia solution was used as the source of ammonia gas.

Emission lifetime data were determined using a customized apparatus (Prof. K. Sakai, Kyushu University) equipped with an Iwatsu DS-4262 digital oscilloscope and a Hamamatsu R928/C3830 photomultiplier tube coupled to a Horiba H-20-VIS grating monochromator. The excitation source was a $N_2$ laser (337 nm) (Usho KEN-1520).

Nitrogen porosity measurements on **α−δ** at 77 K were carried out on a custom-built vacuum line (Prof. I. Gay, Simon Fraser

(30) Leznoff, D. B.; Xue, B.-Y.; Batchelor, R. J.; Einstein, F. W. B.; Patrick, B. O. *Inorg. Chem.* **2001**, *40*, 6026.
(31) Leznoff, D. B.; Lefebvre, J. *Gold Bull.* **2005**, *38*, 47.
(32) Leznoff, D. B.; Xue, B.-Y.; Patrick, B. O.; Sanchez, V.; Thompson, R. C. *Chem. Commun.* **2001**, 259.
(33) Leznoff, D. B.; Xue, B.-Y.; Stevens, C. L.; Storr, A.; Thompson, R. C.; Patrick, B. O. *Polyhedron* **2001**, *20*, 1247.
(34) Schmidbaur, H. *Chem. Soc. Rev.* **1995**, *24*, 391.
(35) Schmidbaur, H. *Gold Bull.* **2000**, *33*, 3.
(36) Pyykkö, P. *Chem. Rev.* **1997**, *97*, 597.
(37) Yam, V. W.-W.; Cheng, E. C.-C. *Top. Curr. Chem.* **2007**, *281*, 269.
(38) Balch, A. L. *Struct. Bonding (Berlin)* **2007**, *123*, 1.
(39) Coker, N. L.; Krause Bauer, J. A.; Elder, R. C. *J. Am. Chem. Soc.* **2004**, *126*, 12.
(40) Assefa, Z.; McBurnett, B. G.; Staples, R. J.; Fackler, J. P., Jr *Inorg. Chem.* **1995**, *34*, 75.
(41) White-Morris, R. L.; Olmstead, M. M.; Balch, A. L. *J. Am. Chem. Soc.* **2003**, *125*, 1033.
(42) Lefebvre, J.; Callaghan, F.; Katz, M. J.; Sonier, J. E.; Leznoff, D. B. *Chem.—Eur. J.* **2006**, *12*, 6748.
(43) Colis, J. C. F.; Larochelle, C.; Staples, R.; Herbst-Irmer, R.; Patterson, H. H. *Dalton Trans.* **2005**, 675.
(44) Assefa, Z.; DeStefano, F.; Garepapaghi, M. A.; LaCasce, J. H., Jr.; Ouellete, S.; Corson, M. R.; Nagle, J. K.; Patterson, H. H. *Inorg. Chem.* **1991**, *30*, 2868.
(45) Hettiarachchi, S. R.; Rawashdeh-Omary, M. A.; Kanan, S. M.; Omary, M. A.; Patterson, H. H.; Tripp, C. P. *J. Phys. Chem. B* **2002**, *106*, 10058.
(46) Nagasundaram, N.; Roper, G.; Biscoe, J.; Chai, J. W.; Patterson, H. H.; Blom, N.; Ludi, A. *Inorg. Chem.* **1986**, *25*, 2947.
(47) Katz, M. J.; Aguiar, P. M.; Batchelor, R. J.; Bokov, A. A.; Ye, Z.-G.; Kroeker, S.; Leznoff, D. B. *J. Am. Chem. Soc.* **2006**, *128*, 3669.
(48) Gründler, P. *Chemical Sensors: An Introduction for Scientists and Engineers*; Springer: Berlin, 2007.
(49) Erxleben, A. *Coord. Chem. Rev.* **2003**, *246*, 203.
(50) Hoskins, B. F.; Robson, R.; Scarlett, N. V. Y. *Angew. Chem., Int. Ed.* **1995**, *34*, 1203.
(51) Lefebvre, J.; Chartrand, D.; Leznoff, D. B. *Polyhedron* **2007**, *26*, 2189.

University) using a gas-volumetric measurement technique. Each sample of **α**−***δ*** was pretreated by heating to 150 °C under vacuum in order to degas the sample and remove any surface-bound solvent. A maximum pressure of 80 Torr was used.

Vapochromic behaviors of the polymorphs **α**−***δ*** were quantified in a customized chamber of known volume. Visible emission spectra were monitored using an Ocean Optics QE65000 spectrometer with an Ocean Optics DH-2000-FHS deuterium/tungsten−halogen source. Both titration and sensitivity limit studies were performed on the different polymorphs by introducing a known amount of $NH_3$ (as a 2.0 M $NH_3$ solution in 2-propanol) into the chamber through a septum using an airtight syringe.

Sensitivities of the different polymorphs to $NH_3$ were determined by sequentially introducing known concentrations of $NH_3$ into the chamber and observing any changes in visible emission at 520 nm. The 520 nm wavelength was chosen in order to ensure that no peak overlap was observed. The emission spectrum of the appropriate $NH_3$-free polymorph starting material was used as the background; this yielded higher sensitivities than use of a MgO white background.

Titration studies were performed by adding sequential equivalents of $NH_3$ per Zn(II) center, allowing the material in the chamber to equilibrate for 30 s, and then measuring the IR spectrum.

**Synthetic Procedures.**

**Caution!** *Although we experienced no difficulties, perchlorate salts are potentially explosive and should be used only in small quantities and handled with care.*

**α-Zn[Au(CN)$_2$]$_2$ (α).** A 15 mL aqueous solution of $KAu(CN)_2$ (57 mg, 0.20 mmol) was added to a 15 mL aqueous solution containing $Zn(ClO_4)_2 \cdot 6H_2O$ (37 mg, 0.10 mmol). Crystals began to form after 2 days of slow, partial evaporation; this process ultimately yielded colorless X-ray-quality crystals of α-Zn[Au(CN)$_2$]$_2$ (**α**). Yield: 40 mg (72%). Anal. Calcd for $C_4N_4Au_2Zn$: C, 8.53; H, 0.00; N, 9.94. Found: C, 8.84; H, 0.00; N, 10.15. IR (KBr): 2216 (w), 2198 (s), 2158 (w), 517 (m) cm$^{-1}$. A similar preparation (using a different stoichiometry) and the crystal structure have been reported previously.[50]

***β*-Zn[Au(CN)$_2$]$_2$ (*β*).** To a 3 mL acetonitrile solution containing $Zn(NO_3)_2 \cdot 6H_2O$ (30 mg, 0.10 mmol) was added a 3 mL acetonitrile solution of $[(n\text{-}Bu)_4N][Au(CN)_2] \cdot {}^1/_2H_2O$ (100 mg, 0.20 mmol) with stirring; this immediately yielded a precipitate. The mixture was centrifuged, after which the solvent was removed and the powder allowed to dry overnight. The sample was washed with three portions of acetonitrile (6 mL) through filter paper to remove any $KNO_3$ or unreacted starting material. The resulting powder was air-dried, yielding a white powder of $\beta$-Zn[Au(CN)$_2$]$_2$ (***β***). Yield: 40 mg (72%). Anal. Calcd for $C_4N_4Au_2Zn$: C, 8.53; H, 0.00; N, 9.94. Found: C, 8.51; H, 0.00; N, 9.78. IR (KBr): 2221 (sh), 2199 (s), 2158 (w), 521 (m) cm$^{-1}$.

X-ray quality crystals of ***β*** were grown by slow, partial evaporation of a 20 mL methanol solution of $KAu(CN)_2$ (57 mg, 0.20 mmol) and $Zn(ClO_4)_2 \cdot 6H_2O$ (37 mg, 0.10 mmol). The crystals and powder had identical IR spectra and powder diffractograms. Crystals of $KClO_4$ were interspersed with crystals of ***β***.

***γ*-Zn[Au(CN)$_2$]$_2$ (*γ*). Method 1.** To a 1 mL acetonitrile solution containing $Zn(ClO_4)_2 \cdot 6H_2O$ (37 mg, 0.10 mmol) was added a 1 mL acetonitrile solution of $[(n\text{-}Bu)_4N][Au(CN)_2] \cdot {}^1/_2H_2O$ (150 mg, 0.30 mmol) dropwise while stirring; this immediately yielded a precipitate. The mixture was centrifuged, after which the solvent was removed and the powder allowed to dry overnight. The sample was washed with three portions of acetonitrile (2 mL) through filter paper to remove any $KClO_4$ and unreacted starting material. The resulting powder was air-dried, yielding a white powder of $\gamma$-Zn[Au(CN)$_2$]$_2$ (***γ***). Yield: 40 mg (72%). Anal. Calcd for $C_4N_4Au_2Zn$: C, 8.53; H, 0.00; N, 9.94. Found: C, 8.62; H, 0.00; N, 9.82. IR (KBr): 2187 (s), 2149 (w), 526 (m) cm$^{-1}$.

**Method 2.** To a 5 mL solution containing $Zn(ClO_4)_2 \cdot 6H_2O$ (37 mg, 0.10 mmol) in 99:1 acetonitrile/water was added a 5 mL solution of $KAu(CN)_2$ (57 mg, 0.20 mmol) in 99:1 acetonitrile/water dropwise while stirring; this immediately yielded a precipitate, which was filtered and washed with three portions of acetonitrile (3 mL), leaving a powder of ***γ***. Yield: 43 mg (77%). The IR spectra and X-ray powder diffractograms of ***γ*** produced by the two methods were identical.

***δ*-Zn[Au(CN)$_2$]$_2$ (*δ*).** A 15 mL aqueous solution containing $KAu(CN)_2$ (114 mg, 0.40 mmol) and KCN (26 mg, 0.40 mmol) was covered with a watch glass and brought to a boil, after which 0.100 N HCl (0.80 mL, 0.080 mmol) was added. The solution was cooled until the beaker was warm to the touch, and then a 15 mL aqueous solution of $ZnCl_2$ (26 mg, 0.20 mmol) was added. Over several hours, crystals of $\delta$-Zn[Au(CN)$_2$]$_2$ (***δ***) were deposited. The crystals were immediately filtered and dried. Yield 60 mg (56%). Anal. Calcd for $C_4N_4Au_2Zn$: C, 8.53; H, 0.00; N, 9.94. Found: C, 8.44; H, 0.00; N, 10.27. IR (KBr): 2191 (s), 2188 (s), 2156 (w), 2151 (w), 526 (m) cm$^{-1}$. Further evaporation yielded a mixture of **α** and ***δ*** crystals, after which a yellow powder of AuCN was produced.

**{Zn(NH$_3$)$_2$[Au(CN)$_2$]$_2$}.** Ammonia gas (10 mL) from the saturated headspace of a bottle of concentrated (29.4%) ammonia solution was introduced into a vial containing 20 mg of ***β***. The vial was sealed and left to stand for 30 min, yielding a white powder. The vial was then opened and the ammonia allowed to escape for 5 min, generating a bright-yellow powder of {Zn(NH$_3$)$_2$[Au(CN)$_2$]$_2$}. Using **α**, ***γ***, or ***δ*** as the starting material also generated {Zn(NH$_3$)$_2$[Au(CN)$_2$]$_2$}. Anal. Calcd for $C_4H_6N_6Au_2Zn$: C, 8.04; H, 1.01; N, 14.07. Found: C, 8.30; H, 0.91; N, 13.87. IR (KBr): 3290 (m), 3178 (w), 2158 (s), 2117 (sh), 1202 (s), 618 (br, m) cm$^{-1}$.

When a sample of {Zn(NH$_3$)$_2$[Au(CN)$_2$]$_2$} was left unsealed for 1 h, a white powder of Zn[Au(CN)$_2$]$_2$ formed. Anal. Calcd for $C_4N_4Au_2Zn$: C, 8.53; H, 0.00; N, 9.94. Found: C, 8.86; H, 0.00; N, 9.80. IR (KBr): 2197 (s), 2160 (w), 518 (m) cm$^{-1}$.

**X-ray Crystallographic Analysis.** Crystallographic data for the four polymorphic compounds **α**−***δ*** and for {Zn(NH$_3$)$_2$[Au(CN)$_2$]$_2$} are provided in Table 1. Crystals of ***β*** and ***δ*** were mounted on glass fibers using epoxy adhesive. The crystals of ***β*** and ***δ*** were colorless plates having dimensions of 0.20 × 0.20 × 0.02 and 0.14 × 0.11 × 0.06 mm, respectively. The data for compounds ***β*** and ***δ*** were collected at room temperature on a Bruker Smart instrument with an APEX II CCD area detector at a distance of 6.0 cm from the crystal. A Mo Kα fine-focus sealed tube operated at 1.5 kW (50 kV, 30 mA) was utilized for data collection. Data for ***β*** and ***δ*** were recorded over 2$\theta$ ranges of 4−57 and 7−65°, respectively.

For compound ***β***, a total of 776 frames were collected with a scan width of 0.5° in $\omega$; all of the frames were collected with an exposure time of 20 s. The frames were integrated with the Bruker SAINT software package. Data were corrected for absorption effects using a numerical face-indexed technique (SADABS) with a transmission range of 0.058−0.700. The final unit-cell dimensions were determined on the basis of the refinement of the *XYZ* centroids of 1969 reflections with 2$\theta$ ranges of 4−51°.

Crystals of compound ***δ*** were determined to be two-component nonmerohedral twins (CELLNOW) by a 180° rotation about the [100] direction in real space. A total of 4079 frames were collected with a scan width of 0.5° in $\omega$; all of the frames were collected with an exposure time of 20 s. Frames were integrated with the Bruker SAINT software package using the appropriate twin matrix. Data were corrected for absorption effects (TWINABS) with a transmission range of 0.036−0.110. The final unit-cell dimensions were determined on the basis of the refinement of the *XYZ* centroids of 9904 reflections with 2$\theta$ ranges of 7−61°

The structures of compounds ***β*** and ***δ*** were solved in CRYSTALS[52] using direct methods (SIR92) and expanded using Fourier techniques. Diagrams were prepared using Cameron.[53]

(52) Betteridge, P. W.; Carruthers, J. R.; Cooper, R. I.; Prout, K.; Watkin, D. J. *J. Appl. Crystallogr.* **2003**, *36*, 1487.
(53) Watkin, D. J.; Prout, C. K.; Pearce, L. J. *Cameron*; University of Oxford Chemical Crystallography Laboratory: Oxford, U.K., 1996.

***Table 1.*** Crystallographic Data for α−***δ*** and $\{Zn(NH_3)_2[Au(CN)_2]_2\}$

| | α[a] | ***β*** | ***γ***[b] | ***δ*** | $\{Zn(NH_3)_2[Au(CN)_2]_2\}$[b] |
|---|---|---|---|---|---|
| empirical formula | $C_4N_4Au_2Zn$ | $C_4N_4Au_2Zn$ | $C_4N_4Au_2Zn$ | $C_4N_4Au_2Zn$ | $C_4H_6N_6Au_2Zn$ |
| formula weight | 563.40 | 563.40 | 563.40 | 563.40 | 597.45 |
| crystal system | hexagonal | monoclinic | tetragonal | monoclinic | tetragonal |
| space group | $P6_422$ | $C2/c$ | $P\bar{4}b2$ | $C2/c$ | $P4_2/mbc$ |
| crystal habit | hexagons | plates | − | crosses | − |
| $a$ (Å) | 8.4520(10) | 8.90060(10) | 6.8208 | 9.9583(3) | 7.8554 |
| $b$ (Å) | 8.4520(10) | 16.8152(2) | 6.8208 | 10.4988(3) | 7.8554 |
| $c$ (Å) | 20.621(11) | 14.3808(2) | 8.4487 | 15.7961(4) | 17.0937 |
| α (deg) | 90 | 90 | 90 | 90 | 90 |
| $\beta$ (deg) | 90 | 100.6000(10) | 90 | 98.407(2) | 90 |
| $\gamma$ (deg) | 120 | 90 | 90 | 90 | 90 |
| $V$ (Å$^3$) | 1275.8(7) | 2115.58(5) | 393.03 | 1633.74(8) | 1054.81 |
| $Z$ | 6 | 8 | 2 | 8 | 4 |
| $T$ (K) | 293 | 293 | 293 | 293 | 293 |
| $\rho_{calcd}$ (g cm$^{-3}$) | 4.400 | 3.537 | 4.760 | 4.581 | 3.724 |
| $\mu$ (mm$^{-1}$) | 37.146 | 29.868 | 40.193 | 38.677 | 29.967 |
| $R$ [$I_o \geq 2.50\sigma(I_o)$][c] | 0.0459 | 0.0429 | 0.0082 | 0.0338 | 0.0366 |
| $R_w$ [$I_o \geq 2.50\sigma(I_o)$][c] | 0.0616 | 0.0564 | 0.0117 | 0.0543 | 0.0691 |
| goodness of fit | − | 1.1438 | − | 1.2462 | − |

[a] From ref 50. [b] From X-ray powder diffraction data. [c] The function minimized was $\sum w(|F_o| - |F_c|)^2$, where $w^{-1} = [\sigma^2(F_o) + (nF_o)^2]$ with $n = 0$ for $\beta$, 0.030 for ***δ***, and 0 for ***γ*** and $\{Zn(NH_3)_2[Au(CN)_2]_2$. $R = \sum||F_o| - |F_c||/\sum|F_o|$; $R_w = [\sum w(|F_o| - |F_c|)^2/\sum w|F_o|^2]^{1/2}$.

***Table 2.*** Bond Lengths (Å) and Angles (deg) for ***β***[a]

| | | | |
|---|---|---|---|
| Zn(1)−N(11) | 1.957(14) | Zn(1)−N(21) | 1.944(15) |
| Zn(1)−N(22) | 1.955(14) | Zn(1)−N(31) | 1.964(13) |
| Au(1)−Au(2*) | 3.2702(6) | Au(1)−Au(2$^{\dagger}$) | 3.2702(6) |
| Au(2′)−Au(3) | 3.1925(7) | Au(2″)−Au(3) | 3.1925(7) |
| Au(2″)−Au(2$^{\dagger}$) | 3.1466(11) | | |
| | | | |
| Zn(1)−N(11)−C(11) | 168.6(16) | Zn(1)−N(21)−C(21) | 171.5(13) |
| Zn(1)−N(22)−C(22) | 162.9(14) | Zn(1)−N(31)−C(31) | 166.6(14) |
| N(11)−Zn(1)−N(21) | 111.4(6) | N(11)−Zn(1)−N(22) | 106.4(6) |
| N(11)−Zn(1)−N(31) | 106.3(6) | N(21)−Zn(1)−N(22) | 112.8(6) |
| N(21)−Zn(1)−N(31) | 108.9(6) | N(22)−Zn(1)−N(31) | 110.8(6) |
| Au(2*)−Au(1)−Au(2$^{\dagger}$) | 180.00 | Au(3$^{\ddagger}$)−Au(2$^{\dagger}$)−Au(1) | 104.944(17) |
| Au(3)−Au(2″)−Au(2$^{\dagger}$) | 145.15(3) | Au(1)−Au(2$^{\dagger}$)−Au(2″) | 109.35(2) |
| Au(2′)−Au(3)−Au(2″) | 141.53(4) | | |

[a] Symmetry operations: (*) $x + {}^1/_2, y + {}^1/_2, z$; (′) $-x + 1, -y + 1, -z$; ($^{\dagger}$) $-x + 2, -y + 1, -z$; ($^{\ddagger}$) $x + 1, y, z$; (″) $x, -y + 1, z - {}^1/_2$.

***Table 3.*** Bond Lengths (Å) and Angles (deg) for ***δ***[a]

| | | | |
|---|---|---|---|
| Zn(1)−N(11) | 1.975(10) | Zn(1)−N(21) | 1.956(10) |
| Zn(1)−N(31) | 1.968(10) | Zn(1)−N(32) | 1.956(10) |
| Au(1)−Au(3′) | 3.3382(5) | Au(1)−Au(3″) | 3.3382(5) |
| Au(2*)−Au(3″) | 3.3318(4) | Au(2*)−Au(3) | 3.3318(4) |
| | | | |
| N(11)−Zn(1)−N(32) | 110.3(4) | N(11)−Zn(1)−N(21) | 113.8(4) |
| N(11)−Zn(1)−N(31) | 100.6(4) | N(21)−Zn(1)−N(31) | 118.9(4) |
| N(21)−Zn(1)−N(32) | 101.2(4) | N(31)−Zn(1)−N(33) | 112.3(5) |
| Zn(1)−N(11)−C(11) | 161.8(10) | Zn(1)−N(21)−C(21) | 163.1(10) |
| Zn(1)−N(31)−C(31) | 158.7(10) | Zn(1)−N(32)−C(32) | 159.3(10) |
| Au(3′)−Au(1)−Au(3″) | 180.00 | Au(3)−Au(2*)−Au(3″) | 180.00 |
| Au(1)−Au(3″)−Au(2*) | 65.690(8) | | |

[a] Symmetry operations: (′) $x - {}^1/_2, y + {}^1/_2, z$; (″) $-x + {}^1/_2, -y + {}^3/_2, -z + 1$; (*) $x, -y + 2, z + {}^1/_2$.

The coordinates and anisotropic temperature factors for all of the atoms of compounds ***β*** and ***δ*** were refined. For ***β***, the final refinement using observed data [$I_o \geq 2.50\sigma(I_o)$] included an extinction parameter, and statistical weights included 103 parameters for 1656 unique reflections. For ***δ***, the final refinement using observed data [$I_o \geq 2.50\sigma(I_o)$] and statistical weights included 104 parameters for 2105 unique reflections. Selected bond lengths and angles are given in Tables 2 and 3, respectively.

X-ray powder diffractograms were collected on a Rigaku RAXIS rapid curved-image plate area detector with a graphite-monochromatized Cu Kα radiation source and a 0.5 $\mu$m collimator. Powder samples were adhered to a glass fiber with grease. Peak positions for ***γ*** and cell parameters were determined with Dicvol.[54] Structural models for ***γ*** were produced and refined with Powder Cell[55] using triclinic symmetry. The space group and atomic positions of the carbon and nitrogen atoms were determined with CRYSTALS[52] using distance and angle restraints. A final refinement cycle for ***γ*** was conducted in Powder Cell[55] in the tetragonal spacegroup $P\bar{4}b2$.

The powder pattern of $\{Zn(NH_3)_2[Au(CN)_2]_2\}$ was compared with simulated patterns for the coordination polymer $\{Cd(NH_3)_2[Ag(CN)_2]_2\}$,[56] which was found to have a similar diffraction pattern. The unit-cell determination and susbsequent refinements were performed in Powder Cell[55] using the atomic positions for the $\{Cd(NH_3)_2[Ag(CN)_2]_2\}$ complex.[56] The relative

(54) Boultif, A.; Louer, D. *J. Appl. Crystallogr.* **2004**, *37*, 724.
(55) Kraus, W.; Nolze, G. *J. Appl. Crystallogr.* **1996**, *29*, 301.
(56) Soma, T.; Iwamoto, T. *Chem. Lett.* **1995**, 271.

intensities of the 21*l* reflections in the observed powder pattern were consistently less intense and very broad in comparison with those in the calculated powder diffractogram.

## Results and Discussion

**Synthesis and IR Spectra.** Studies of the physical properties associated with $M(H_2O)_n[Au(CN)_2]_2$ systems [M = Cu(II), Ni(II), Pb(II); $n$ = 1, 2] have yielded interesting magnetic,[42] vapochromic,[17] and birefringent materials.[47] As an analogue to the vapochromic, green Cu(II) system, we targeted the related $d^{10}$ Zn(II)-containing material, as the geometry of the Zn(II) cation shows flexibility similar to that of Cu(II).[49] Although the synthesis and structure of $Zn[Au(CN)_2]_2$ was reported previously,[50] no luminescence or further characterization was described. In our efforts to investigate this system with the goal of measuring its luminescence and potentially harnessing it as a vapoluminescent sensor, we discovered that the structure of the deceptively simple $Zn[Au(CN)_2]_2$ material has an exquisite sensitivity to synthetic conditions. Thus, exploration of the reaction of Zn(II) salts with 2 equiv of the linear anionic $Au(CN)_2^-$ building block resulted in the controllable formation of *four* polymorphs, **α**−***δ***, of $Zn[Au(CN)_2]_2$ (eqs 1–4):

$$ZnX_2 + 2KAu(CN)_2 \xrightarrow[X = Cl^-, NO_3^-, ClO_4^-]{30\ mL\ H_2O} \alpha\text{-}Zn[Au(CN)_2]_2(cryst) \quad (1)$$

$$Zn(NO_3)_2 + 2[(n\text{-}Bu)_4N][Au(CN)_2] \xrightarrow[2.\ -CH_3CN\ (24\ h,\ RT)]{1.\ 6\ mL\ CH_3CN} \beta\text{-}Zn[Au(CN)_2]_2(ppt) \quad (2)$$

$$Zn(ClO_4)_2 + 2KAu(CN)_2 \xrightarrow{10\ mL\ CH_3CN} \gamma\text{-}Zn[Au(CN)_2]_2(ppt) \quad (3)$$

$$2KAu(CN)_2 + 2KCN \xrightarrow[3.\ Cool\ to\ 50\ °C;\ 4.\ ZnCl_2]{1.\ \Delta\ (100\ °C);\ 2.\ 0.4\ HCl} \delta\text{-}Zn[Au(CN)_2]_2(cryst) \quad (4)$$

All four materials had comparable elemental analyses and thus are true polymorphs rather than pseudopolymorphic solvent adducts.[57]

The synthesis of each polymorph was sensitive to solvent choice,[58–61] concentration,[17,62] pH,[63,64] and even the counterions associated with either the Zn(II) or Au(I) starting material, despite the fact that these counterions are not incorporated into the final polymer. This last point is best exemplified by comparing the syntheses of ***β*** and ***γ*** (eqs 2 and 3), where changing the counterion of Au(I) from $K^+$ to $[(n\text{-}Bu)_4N]^+$ and the counterion of Zn(II) from $NO_3^-$ to $ClO_4^-$ generated ***γ*** instead of ***β*** under similar reaction conditions. Furthermore, when only one counterion was changed, a mixture of polymorphs ***β*** and ***γ*** was obtained. The counterions in the synthesis of ***β*** and ***γ*** could play an important role as a templating agent, preferentially inducing the formation of one network versus another.[2]

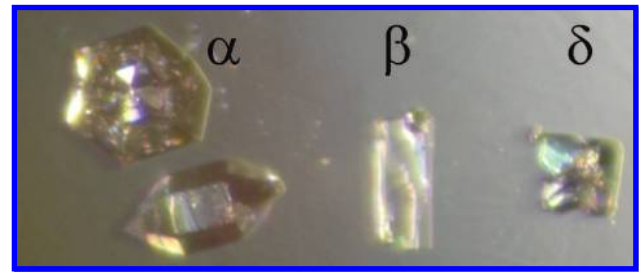


***Figure 1.*** Habit of polymorph crystals: (left) two hexagonal crystals of **α**; (middle) plate-shaped crystal of ***β***; (right) cross-shaped crystal of ***δ***, in which each arm of the cross is a two-component nonmerohedral twin.

Conversely, the synthetic route to **α** was insensitive to counterions and moderately insensitive to concentration, although mixtures of **α** and ***δ*** were formed under extremely concentrated conditions (2 mL total). Changing the solvent in eq 1 from water to methanol produced only crystals of ***β*** when $Zn(ClO_4)_2$ was used (See the Experimental Section). The difference may be partially attributed to differences in the hydrogen-bonding characteristics of water and methanol.[65] The same effect was also observed in the synthesis of ***δ***, which was performed under acidic conditions (eq 4) with $ZnCl_2$.

While the rationale behind the preferential formation of a particular polymer under a defined set of conditions is unclear, it is obvious from eqs 1–4 that the formation constant for each polymorph is relatively similar. Changing the solvent, concentration, counterion, and/or pH is sufficient to easily shift the resultant energy minimum from one polymorphic form to another.

The IR spectra of all four polymorphs **α**−***δ*** are similar, having strong $\nu_{CN}$ stretch peaks between 2187 and 2199 $cm^{-1}$ with readily visible $^{13}C$ satellites between 2158 and 2149 $cm^{-1}$. These bands are all shifted to higher energy relative to those for $KAu(CN)_2$ ($\nu_{CN}$ = 2141 $cm^{-1}$), indicating that all of the cyanide groups are bound to a zinc center.[29] For the most part, the similarities in the IR spectra for **α**−***δ*** precluded the use of the IR signatures as a definitive polymorph identifier; this identification was accomplished on the basis of a combination of distinct crystal habits (Figure 1), X-ray powder diffractograms, and emission data (see below).

**Crystal Structures of the Polymorphs. Crystal Structure of α-Zn[Au(CN)$_2$]$_2$.** The synthesis of **α** using a $Zn/Au(CN)_2$ ratio of 3:1 and the crystal structure of the resulting hexagonal crystals were previously reported.[50] In our work, the stoichiometrically rational reaction of Zn(II) and 2 equiv of $KAu(CN)_2$ in water generated the same hexagonal crystals (Table 1 and Figure 1); the crystal structure is briefly described below for comparative purposes. The crystal structure of **α** contains a zinc center with four N-bound cyanides (Zn−N bond lengths of 1.939 and 1.978 Å) in a tetrahedral geometry, thereby generating a three-dimensional (3D) coordination polymer. The network structure of **α** consists of corner-sharing tetrahedra analogous to those in

(57) Elemental analysis indicated that when ***β*** was initially formed (eq 2), it contained at least one labile acetonitrile per $Zn[Au(CN)_2]_2$ unit. This complex readily desolvated when left in an unsealed container overnight. Powder X-ray diffractograms showed no difference between the solvated and desolvated forms of ***β***.

(58) Parmar, M. M.; Khan, O.; Ford, J. L. *Cryst. Growth Des.* **2007**, *7*, 1635.
(59) Blagus, A.; Kaitner, B. *J. Chem. Crystallogr.* **2007**, *37*, 473.
(60) Katz, M. J.; Shorrock, C. J.; Batchelor, R. J.; Leznoff, D. B. *Inorg. Chem.* **2006**, *45*, 1757.
(61) Blake, A. J.; Brooks, N. R.; Champness, N. R.; Crew, M.; Deveson, A.; Fenske, D.; Gregory, D. H.; Hanton, L. R.; Hubberstey, P.; Schröder, M. *Chem. Commun.* **2001**, 1432.
(62) Lu, J.; Wang, X.-J.; Yang, X.; Ching, C.-B. *Cryst. Growth Des.* **2007**, *7*, 1590.
(63) Lee, I. S.; Kim, K. T.; Lee, A. Y.; Myerson, A. S. *Cryst. Growth Des.* **2008**, *8*, 108.
(64) Mølgaard, A.; Larsen, S. *Acta Crystallogr.* **2004**, *D60*, 472.
(65) Zaworotko, M. J. *Chem. Soc. Rev.* **1994**, *23*, 283.

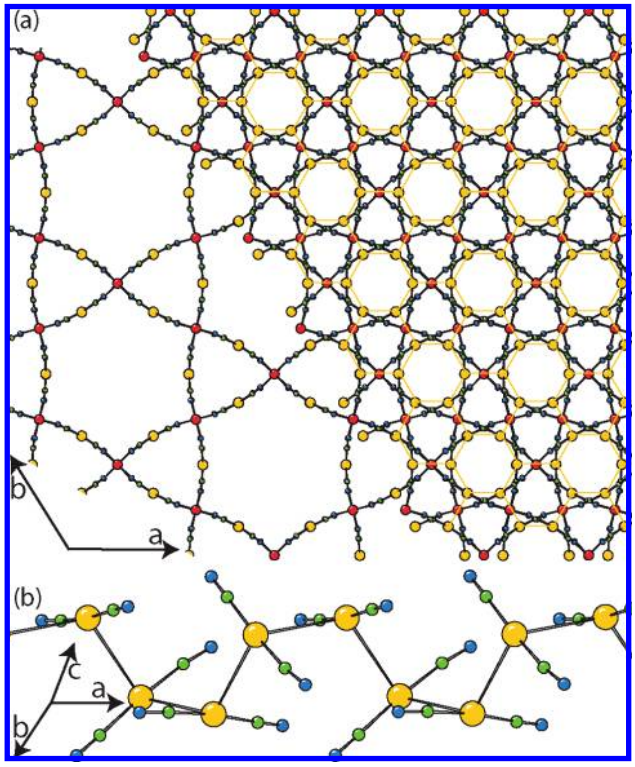


***Figure 2.*** (a) Crystal structure of **α** viewed down the *c* axis: (left) a single quartz-like network; (right) all six interpenetrated quartz-like networks. (b) 1D chain of gold−gold-bonded $Au(CN)_2^-$ units. Color scheme: Au, yellow; Zn, red; N, blue; C, green.

$SiO_2$ quartz (Figure 2a);[66–70] each tetrahedron is defined by a Au(I) atom at each vertex and a Zn(II) atom at the center. In order to efficiently utilize the large space between neighboring zinc centers in this quartz-type net, the structure is sixfold-interpenetrated (Figure 2a, right).[68,69] The interpenetration is supported via gold−gold bonds having alternating lengths of 3.11 and 3.16 Å, forming a 1D zigzag chain of $Au(CN)_2^-$ units with Au−Au−Au angles of 114.98° (Figure 2b). A similar structure was reported for $Co[Au(CN)_2]_2$.[71]

**Crystal Structure of *β*-$Zn[Au(CN)_2]_2$.** Rectangular plate crystals of ***β*** (Figure 1) were obtained from partial evaporation of a methanol solution of $Zn(ClO_4)_2$ and $KAu(CN)_2$. Like that of **α**, the crystal structure of ***β*** also consists of a Zn(II) center surrounded by four N-bound cyanide groups in a tetrahedral geometry with Zn−N bond lengths of 1.941(14)−1.961(14) Å (Table 1). The tetrahedra are corner-sharing, this time forming a 3D structure having a diamond-type topology;[65,68,69,72–74] each building block in the network can be viewed as an adamantoid unit (Figure 3a). The framework is analogous to that of

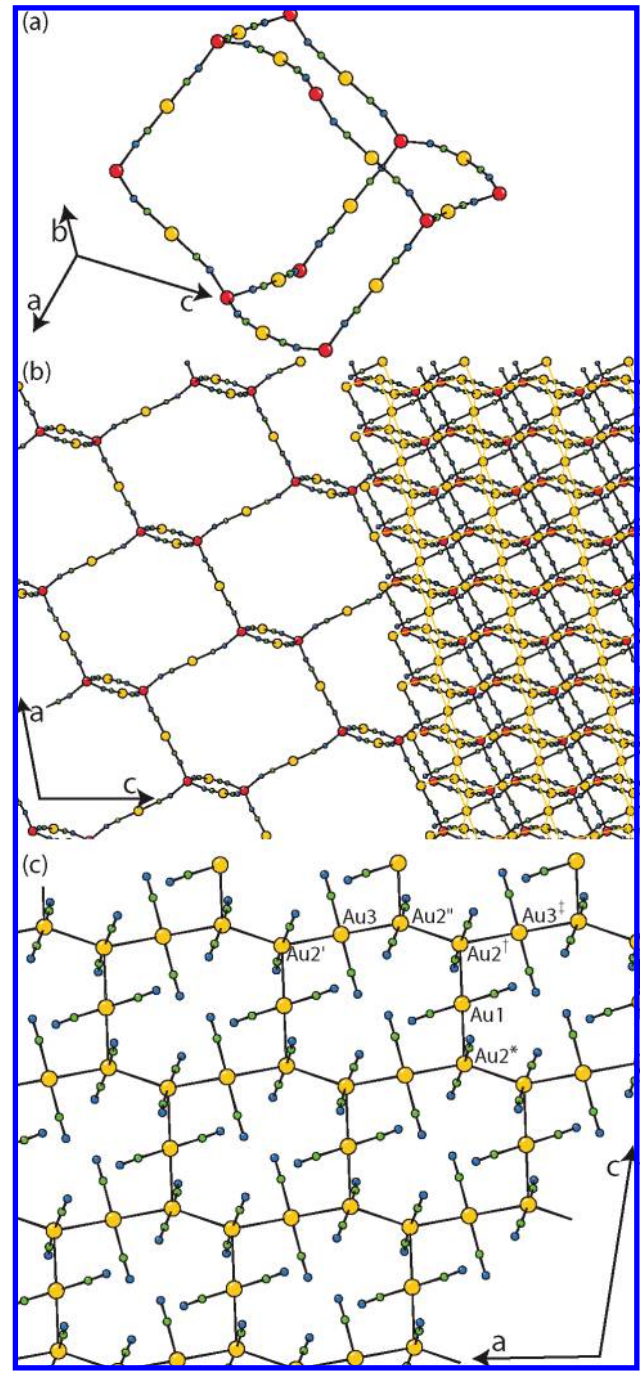


***Figure 3.*** Crystal structure of ***β***. (a) One diamond-like repeat unit. (b) (left) One diamond-like network viewed down the *b*-axis; (right) all five interpenetrated networks. (c) Distorted hexagonal 2D (6, 3) network of gold−gold-bonded $Au(CN)_2^-$ units. Color scheme: Au, yellow; Zn, red; N, blue; C, green.

cristobalite, another polymorph of $SiO_2$ (Figure 3).[70] The 3D networks in ***β*** are fivefold-interpenetrated (Figure 3b, right).[68,69,73] The interpenetrated networks are linked via gold−gold bonds having lengths in the range 3.1471(11)−3.2702(6) Å and forming angles in the range 104.951(17)−180° (Table 2 and Figure 3c). Whereas the aurophilic array of **α** forms 1D chains of Au centers, the Au array in ***β*** forms a 2D (6, 3) network[68] in which the gold atoms form distorted hexagonal motifs with gold atoms located at the vertices and at the midpoints of four of the sides of the hexagons (Figure 3c).

(66) Sun, J.; Weng, L.; Zhou, Y.; Chen, J.; Chen, Z.; Liu, Z.; Zhao, D. *Angew. Chem., Int. Ed.* **2002**, *41*, 4471.
(67) Hu, S.; Tong, M.-L. *Dalton Trans.* **2005**, 1165.
(68) Batten, S. R.; Robson, R. *Angew. Chem., Int. Ed.* **1998**, *37*, 1460.
(69) Öhrström, L.; Larsson, K. *Molecule-Based Materials: The Structural Network Approach*; Elsevier: Amsterdam, 2005.
(70) Wenk, H.-R.; Bulakh, A. *Minerals: Their Constitution and Origin*; Cambridge University Press: Cambridge, U.K., 2004.
(71) Abrahams, S. C.; Zyontz, L. E.; Bernstein, J. L. *J. Chem. Phys.* **1982**, *76*, 5458.
(72) Moulton, B.; Zaworotko, M. J. *Chem. Rev.* **2001**, *101*, 1629.
(73) Blatov, V. A.; Carlucci, L.; Ciani, G.; Proserpio, D. M. *CrystEngComm* **2004**, *6*, 377.
(74) Proserpio, D. M.; Hoffmann, R.; Preuss, P. *J. Am. Chem. Soc.* **1994**, *116*, 9634.

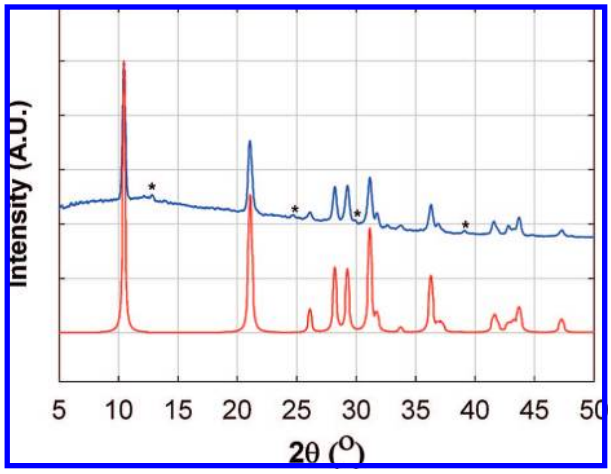


***Figure 4.*** Simulated (red) and observed (blue) powder diffractograms for $\gamma$. Peaks labeled with * arise from a small (3%) $\alpha$ impurity.

**Crystal Structure of $\gamma$-Zn[Au(CN)$_2$]$_2$.** Although single crystals of $\gamma$ could not be obtained, a pure microcrystalline powder of $\gamma$ was synthesized from $Zn(ClO_4)_2$ and [cation][$Au(CN)_2$] [cation = $K^+$, ($n$-Bu)$_4N^+$] in MeCN. The powder diffractogram of $\gamma$ was observed to be similar to that for the previously reported Pb[$Au(CN)_2$]$_2$ structure.[47] Using this Pb(II) structure as a starting model, we determined the structure of $\gamma$ from powder X-ray diffraction data. An excellent match between the predicted and experimental powder diffractograms (Figure 4) was obtained. The structure is both chemically reasonable and spectroscopically consistent. Interestingly, the crystal structure of $\gamma$ has the same network structure as $\beta$: a diamond-type array formed by fused adamantoid units (Figures 3a and 5).[65,68,69,72–74]

There are several differences between these polymorphs. First, the networks of $\gamma$ are fourfold-interpenetrating (Figure 5b), while $\beta$ contains five independent networks (Figure 3c).[68,73] The interpenetration in $\gamma$ is supported by gold−gold bonds having lengths of 3.29 Å. However, in contrast to the 2D array of gold atoms present in $\beta$, the gold atoms in $\gamma$ primarily form dimers. Long-distance (3.58 Å) gold−gold interactions link the dimers to one another (Figure 5b). In addition, the shape of the diamond network in $\gamma$ is more prolate than that in $\beta$. A single adamantoid framework in $\beta$ has dimensions of 25.8 × 16.5 × 13 Å (Figure 3a), while an adamantoid framework in $\gamma$ has dimensions of 33.8 × 9.6 × 9.6 Å (Figure 5).

**Crystal Structure of $\delta$-Zn[Au(CN)$_2$]$_2$.** Twinned cross-shaped crystals of $\delta$ (Figure 1) were obtained from an acidic aqueous solution containing $ZnCl_2$, $KAu(CN)_2$, and KCN; this synthesis was a modified form of the one given in an old report on Zn/$Au(CN)_2$ reactivity that did not identify any of the polymorphs.[75] As in $\alpha$−$\gamma$, the crystal structure of $\delta$ contains tetrahedral zinc centers with Zn−$N_{cyano}$ bond lengths ranging from 1.956(10) to 1.986(10) Å. However, while $\alpha$, $\beta$, and $\gamma$ form easily recognizable structures based on corner-sharing tetrahedra, the 3D structure of $\delta$ is considerably more complicated. Temporarily omitting one of the $Au(CN)_2^-$ units on each zinc center [the $Au(CN)_2^-$ unit containing Au(3)], the structure can be simplified to a corrugated 2D (6, 3) herringbone structure (Figure 6a,b) along the (10$\bar{1}$) plane.[68,72] A second (6, 3) herringbone network is interwoven through the first (Figure 6b, right). Long gold−gold distances of 3.6430(9) Å represent the only close contacts between these two networks. Via the previously omitted

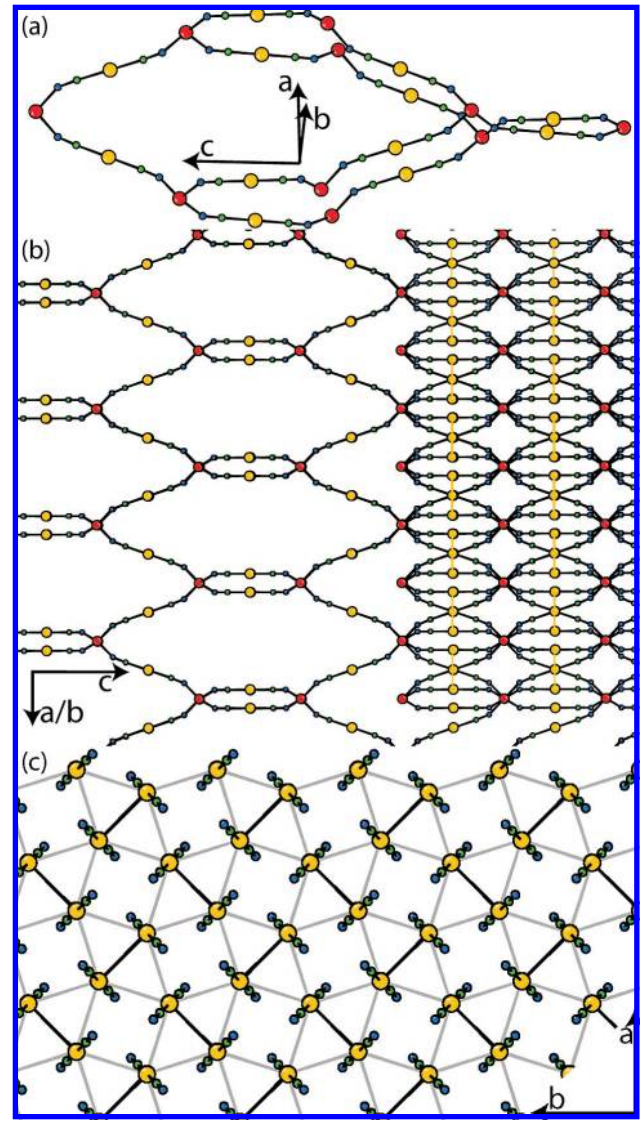


***Figure 5.*** Crystal structure of $\gamma$. (a) One diamond-like repeat unit. (b) (left) Single diamond-like framework; (right) All four interpenetrated networks. (c) Network of gold−gold bonded $Au(CN)_2^-$ units containing $Au(CN)_2^-$ dimers (Au−Au distance of 3.29 Å) connected via longer Au−Au interactions (Au−Au distance of 3.58 Å). Color scheme: Au, yellow; Zn, red; N, blue; C, green.

$Au(CN)_2^-$ unit, each individual herringbone network is linked to four additional networks, namely, the pair of interwoven networks above and the pair of networks below, completing the basic 3D structure (Figure 6c, left). The void space is filled by two additional identical 3D interpenetrated networks (Figure 6c, right).[68] The interpenetration is supported via gold−gold bonds having lengths of 3.3318(4) and 3.3382(5) Å (Figure 6d). The gold−gold bonds in $\delta$ are longer then those observed in $\alpha$, $\beta$, and $\gamma$.

Polymorphism has been extensively investigated in coordination polymers, and structural differences between polymorphic forms have been attributed to connectivity, interpenetration, and degree of solvent inclusion (pseudopolymorphism).[61,72,76–79]

(75) Feldtmann, W. B. *J. Chem., Metall. Min. Soc. S. Afr.* **1919**, *20*, 13.
(76) Bernstein, J.; Davey, R. J.; Henck, J.-O. *Angew. Chem., Int. Ed.* **1999**, *38*, 3440.
(77) Dunitz, J. D.; Bernstein, J. *Acc. Chem. Res.* **1995**, *28*, 193.
(78) Blagden, N.; Davey, R. J. *Cryst. Growth Des.* **2003**, *3*, 873.
(79) Gavezzotti, A. *CrystEngComm.* **2002**, *4*, 343.

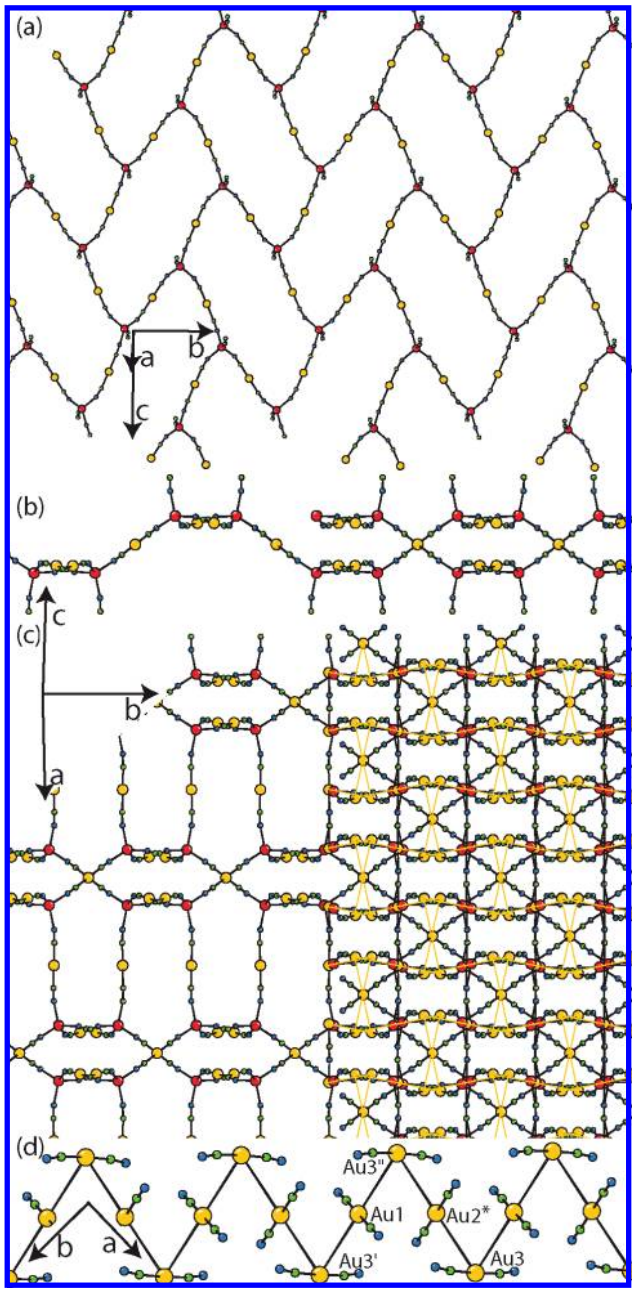


***Figure 6.*** Crystal structure of ***δ***. (a) One herringbone network. (b) (left) Side view of herringbone network; (right) pair of interwoven herringbone networks. (c) (left) One full 3-D network; (right) all three interpenetrated networks. (d) 1D chain of gold−gold-bonded $Au(CN)_2^-$ units. Color scheme: Au, yellow; Zn, red; N, blue; C, green.

Even the widely investigated prototypical Prussian Blue-like system, $Mn[Fe(CN)_6]$, has been observed in two polymorphic forms: the standard rock-salt structure and the doubly interpenetrated form.[80]

In the case of the four polymorphs **α**−***δ***, all have zinc centers in a tetrahedral geometry. The difference between the networks of **α** and ***δ*** and the diamond-like networks of ***β*** and ***γ*** lies in the pathways connecting zinc centers. Furthermore, the four polymorphs differ in the degree of interpenetration, which decreases from sixfold to threefold in going from **α** to ***δ***. In all of the polymers, the interpenetration is supported by gold−gold bonds ranging from 3.11−3.34 Å. While it is generally believed that a lower degree of interpenetration is ideal for creating empty cavities,[65] it is interesting to note that ***β*** has a significantly lower density then the other polymorphs, despite the relatively high degree of interpenetration.[81–83]

***Table 4.*** Summary of Luminescence Data for **α**−***δ***, $[Zn(NH_3)_4][Au(CN)_2]_2$, and $\{Zn(NH_3)_2[Au(CN)_2]_2\}$

| compound | emission maximum (nm) | excitation maximum (nm) |
|---|---|---|
| **α** | 390, 480 | 345 |
| ***β*** | 450 | 390 |
| ***γ*** | 440 | 360 |
| ***δ*** | none | none |
| $[Zn(NH_3)_4][Au(CN)_2]_2$ | 430 | 365 |
| $\{Zn(NH_3)_2[Au(CN)_2]_2\}$ | 500 | 400 |

**Thermal Stability.** All four polymorphs are stable at temperatures below 350 °C, above which they begin to decompose, losing all of the cyanide groups in one step between 350−390 °C. Thus, despite the different levels of interpenetration and supporting gold−gold networks, the four polymorphs show very similar thermal stabilities. In addition, DSC measurements of **α**−***δ*** over a temperature range of 25−300 °C showed no indication of phase changes from one polymorph to another.

**Photoluminescence.** Au(I) centers separated by less than 3.6 Å (twice the van der Waals radius for gold)[84] are said to show gold−gold (aurophilic) bonding;[34,85] such systems are known to be potentially luminescent.[37,38] As a result of their interesting emission properties, compounds containing gold−gold bonds have received a great deal of attention.[36,37,45,46,86–89] In the crystal structures of **α**−***δ***, network interpenetration is supported via gold−gold bonds with lengths of 3.11−3.34 Å, and indeed, **α**−***γ*** are emissive when exposed to UV light at room temperature.

Data from the room-temperature photoluminescence spectra of **α**−***δ*** are summarized in Table 4. Compound **α** shows two emission bands at 390 and 480 nm (Figure 7). The excitation spectrum of **α** shows an identical excitation maximum at 345 nm for both of the emission bands (Figure 7, bottom). However, for crystals or densely packed powder samples of **α**, the 480 nm emission band can be directly excited at 390 nm. The lifetimes of the two emissions were measured in order to determine the natures of the emissions. The 390 nm emission has a lifetime of 240 ns, while the 480 nm emission has a lifetime of 930 ns. On the basis of these data and the lifetimes of other $Au(CN)_2^-$-based coordination polymers,[90,91] the 390 and 480 nm emissions were assigned to singlet (fluorescence) and triplet (phosphorescence) emissions, respectively. Due to the large spin−orbit coupling in gold, phosphoresence is

(80) Buschmann, W. E.; Miller, J. S. *Inorg. Chem. Commun.* **1998**, *1*, 174.
(81) Cartraud, P.; Cointot, A.; Renaud, A. J. *J. Chem. Soc., Faraday Trans.* **1981**, *77*, 1561.
(82) Chomič, J.; Čèrnák, J. *Thermochim. Acta* **1985**, *93*, 93.
(83) Evans, O. R.; Lin, W. *Acc. Chem. Res.* **2002**, *35*, 511.
(84) Bondi, A. *J. Phys. Chem.* **1964**, *68*, 441.
(85) Bardají, M.; Laguna, A. *J. Chem. Educ.* **1999**, *76*, 201.
(86) Stender, M.; Olmstead, M. M.; Balch, A. L.; Rios, D.; Attar, S. *Dalton Trans.* **2003**, 4282.
(87) Pham, D. M.; Rios, D.; Olmstead, M. M.; Balch, A. L. *Inorg. Chim. Acta* **2005**, *358*, 4261.
(88) Fackler, J. P., Jr *Inorg. Chem.* **2002**, *41*, 6959.
(89) Rawashdeh-Omary, M. A.; Omary, M. A.; Patterson, H. H., Jr *J. Am. Chem. Soc.* **2001**, *123*, 11237.
(90) Hettiarachchi, S. R.; Schaefer, B. K.; Yson, R. L.; Staples, R. J.; Herbst-Irmer, R.; Patterson, H. H. *Inorg. Chem.* **2007**, *46*, 6997.
(91) Arvapally, R. K.; Sinha, P.; Hettiarachchi, S. R.; Coker, N. L.; Bedel, C. E.; Patterson, H. H.; Elder, R. C.; Wilson, A. K.; Omary, M. A. *J. Phys. Chem. C* **2007**, *111*, 10689.

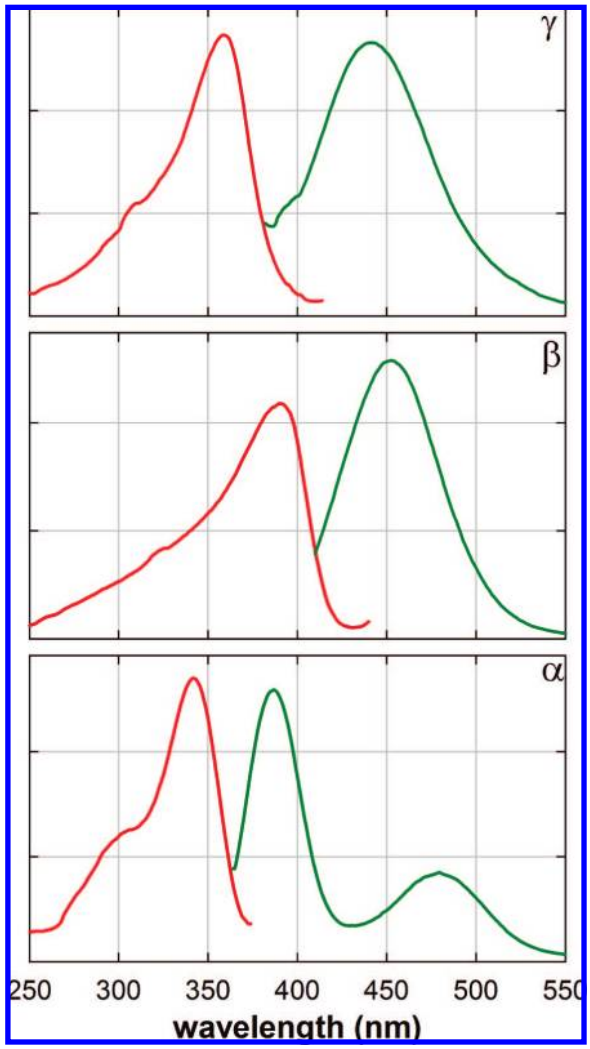


***Figure 7.*** Excitation (red) and emission (green) spectra of (bottom) **α**, (middle) ***β***, and (top) ***γ***.

generally the predominant emission pathway. The presence of both types of emission, as in **α**, is less common.[91]

In contrast, ***β*** and ***γ*** each show only one emission band; these bands have similar emission maxima (450 and 440 nm, respectively) (Table 4 and Figure 7). Despite the presence of gold−gold bonds, hand-picked single crystals of ***δ*** showed no observable room-temperature luminescence. The absorption spectra of **α**−***γ*** showed that the lowest-energy absorption band is consistent with the lowest fluorescence excitation energy, confirming that the observed emissions are attributed to the polymorphs. Other $Au(CN)_2^-$-based coordination polymers have also shown excitation and emission energies in this range.[43,45,86,89,92]

It has been observed both theoretically and experimentally that the gold−gold distances in a structurally related series of metal−metal-bonded Au(I) systems are inversely proportional to the emission energies.[39,40,46] Indeed, the low-energy phosphoresence emissions of **α**−***γ*** obey this trend; on average, the shorter gold−gold bonds in **α** (3.11 and 3.16 Å) emit at higher energy than the gold−gold bonds in ***β*** [3.1471(11)−3.2702(6) Å] and ***γ*** (3.29 Å). A plot of the average Au−Au distance versus emission energy (Figure S3 in the Supporting Information) yields a straight line and also predicts that ***δ*** should emit at 427 nm. However, a nonemissive decay pathway may be more prevalent in ***δ*** at room temperature.

**Response to Ammonia Exposure.** On the basis of the sensitive and dramatic visible and IR spectral response of the related $Cu(H_2O)_2[Au(CN)_2]_2$ system to ammonia gas,[17] the response of the colorless polymorphs **α**−***δ*** to ammonia vapor was examined, with a particular focus on possible emission changes acting as a sensory output. Ammonia detectors have a variety of applications in agriculture, the automotive industry, industrial refrigeration, medical diagnosis, and antiterrorism.[93] Also, from a health perspective, the human nose is capable of sensing ammonia at a concentration of 50 ppm, which is higher than the permissible long-term exposure limit of 20 ppm for ammonia.[93,94] For these reasons, the design of materials for the detection of ammonia is of great interest.

Exposing the four polymorphs **α**−***δ*** to a large excess of $NH_3$ gas produced a new white powder whose IR spectrum contained only one $\nu_{CN}$ band at 2141 $cm^{-1}$, indicative of free $Au(CN)_2^-$ units. The IR spectrum also showed the presence of metal-bound ammonia,[95] suggesting that the Zn(II) center is either tetrahedrally or octahedrally coordinated by ammonia; the former is more likely on the basis of typical Zn(II)−ammine coordination chemistry,[96,97] and therefore, this ammonia-saturated powder is tentatively assigned the formula $[Zn(NH_3)_4][Au(CN)_2]_2$. The room-temperature luminescence spectrum of this ammonia-saturated complex shows a single emission peak at 430 nm with an excitation band at 365 nm (Figure 8). Unfortunately, rapid loss (over a few seconds) of some of the ammonia occurred when the sample is unsealed, precluding further structural or elemental analysis.

Removal from the ammonia-rich atmosphere and subsequent rapid loss of excess ammonia from $[Zn(NH_3)_4][Au(CN)_2]_2$ generated a yellow powder (Figure 9) that was stable in the absence of ammonia for 30 min. Elemental analysis of this yellow powder was consistent with a bis(ammonia) adduct of $Zn[Au(CN)_2]_2$, namely $\{Zn(NH_3)_2[Au(CN)_2]_2\}$. The IR spectrum of this compound shows a single $\nu_{CN}$ band at 2158 $cm^{-1}$, suggesting that all of the $Au(CN)_2^-$ units occupy a similar environment. Furthermore, the vibrational modes associated with the ammonia molecule suggest the presence of a metal-bound ammine.[95] Comparison of the powder X-ray diffractogram of $\{Zn(NH_3)_2[Au(CN)_2]_2\}$ to those of other closely related bis(ammonia) coordination polymers[56,92,99,100] revealed similarities to the diffractograms of $\{Cd(NH_3)_2[Ag(CN)_2]_2\}$[56] and $\{Cu(NH_3)_2[Ag(CN)_2]_2\}$.[100] The powder pattern of the cadmium

(92) Stender, M.; White-Morris, R. L.; Olmstead, M. M.; Balch, A. L. *Inorg. Chem.* **2003**, *42*, 4504.
(93) Timmer, B.; Olthuis, W.; van den Berg, A. *Sens. Actuators, B* **2005**, *107*, 666.
(94) Budarvari, S.; O'Neil, M. J.; Smith, A.; Heckelman, P. E.; Kinneary, J. F. *The Merck Index*, 12th ed.; Merck: Rahway, NJ, 1996.
(95) Nakamoto, K. *Infrared and Raman Spectra of Inorganic and Coordination Compounds*, 5th ed.; Wiley: New York, 1986.
(96) Migdał-Mikuli, A.; Mikuli, E.; Hetmańczyk, Ł.; Natkaniec, I.; Hołderna-Natkaniec, K.; Łasocha, W. *J. Solid State Chem.* **2003**, *174*, 357.
(97) Hillebrecht, H.; Thiele, G.; Koppenhöfer, A.; Vahrenkamp, H. *Z. Naturforsch., B.* **1994**, *49*, 1163.
(98) Prince, R. H. In *Comprehensive Coordination Chemistry*; Wilkinson, G., Gillard, R. D., McCleverty, J., Eds.; Pergamon Press: Oxford, U.K., 1987.
(99) Suárez-Varela, J.; Sakiyama, H.; Cano, J.; Colacio, E. *Dalton Trans.* **2007**, 249.
(100) Vlček, A.; Orendáč, M.; Orendáčová, A.; Kajňaková, M.; Papageorgiou, T.; Chomič, J.; Černák, J.; Massa, W.; Feher, A. *Solid State Sci.* **2007**, *9*, 116.

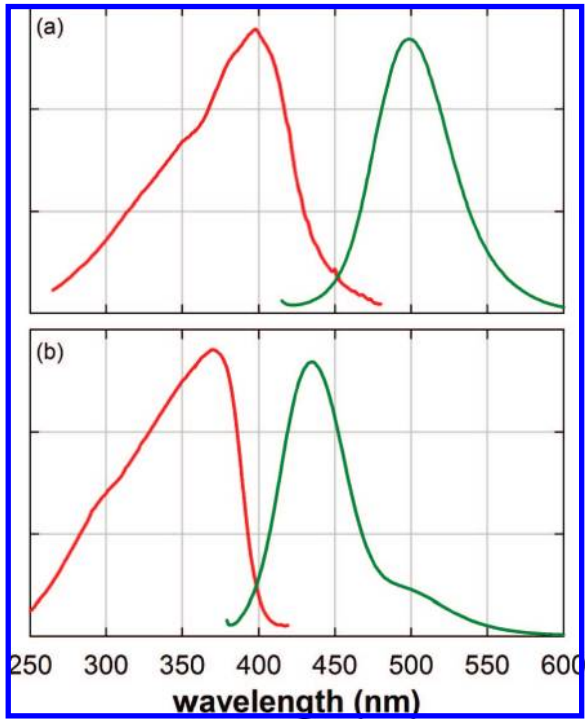


***Figure 8.*** Excitation and emission spectra of (a) $\{Zn(NH_3)_2[Au(CN)_2]_2\}$ and (b) fully saturated $[Zn(NH_3)_4][Au(CN)_2]_2$.

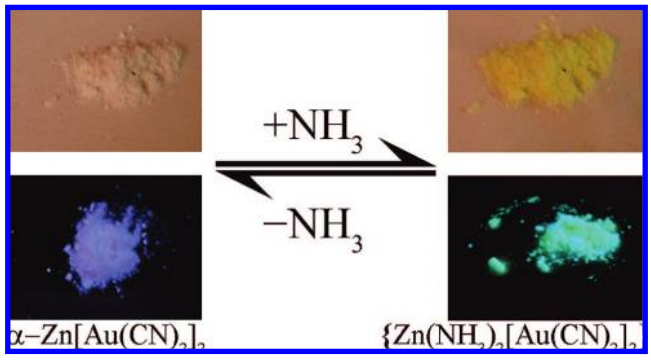


***Figure 9.*** (left) Powder of α under (top) visible light and (bottom) UV. Exposure to ammonia (right) yields (top) the yellow compound $\{Zn(NH_3)_2[Au(CN)_2]_2\}$ with (bottom) bright green luminescence.

polymer is a better fit, which is consistent with the fact that neither Zn(II) nor Cd(II) contains the Jahn−Teller axis present in the Cu(II) system. With the Cd(II) system as a starting model, the solid-state structure of $\{Zn(NH_3)_2[Au(CN)_2]_2\}$ was determined by fitting atomic coordinates to the experimental powder X-ray diffraction pattern. A good match was obtained (Figure 10), except for the reflections from the $\{21l\}$ planes. These planes intersect Zn atoms, making them sensitive to gain or loss of $NH_3$; therefore, their reflections are much broader than the other peaks. Consistent with the IR data, the structure contains an octahedral zinc center with $D_{4h}$ geometry having trans-oriented ammonia molecules and four N-bound cyanides. Linking through the $Au(CN)_2^-$ units, the zinc centers form a 2D corrugated sheet (Figure 11a)[68,69] with $Au(CN)_2^-$ units at the apexes of the corrugation.[56]Additional parallel sheets stack via gold−gold bonds having lengths of 3.06 Å (Figure 11b). Instead of chains or sheets of gold−gold bonds like those in **α**, ***β***, and ***δ***, only discrete dimers of $Au(CN)_2^-$ units similar

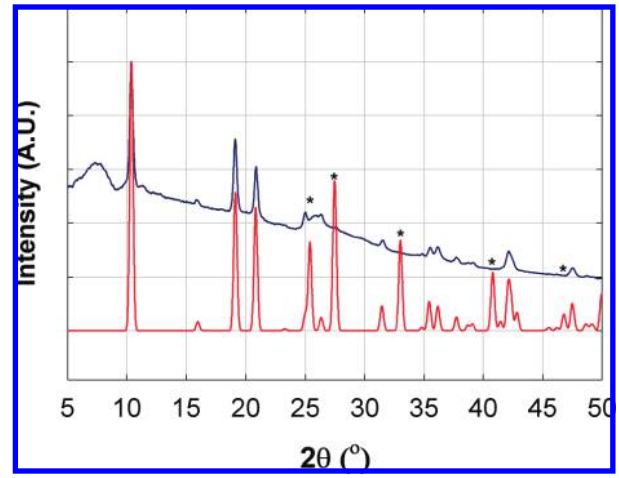


***Figure 10.*** Simulated (red) and observed (blue) powder diffractograms of $\{Zn(NH_3)_2[Au(CN)_2]_2\}$. The * labels indicate $21l$ reflections.

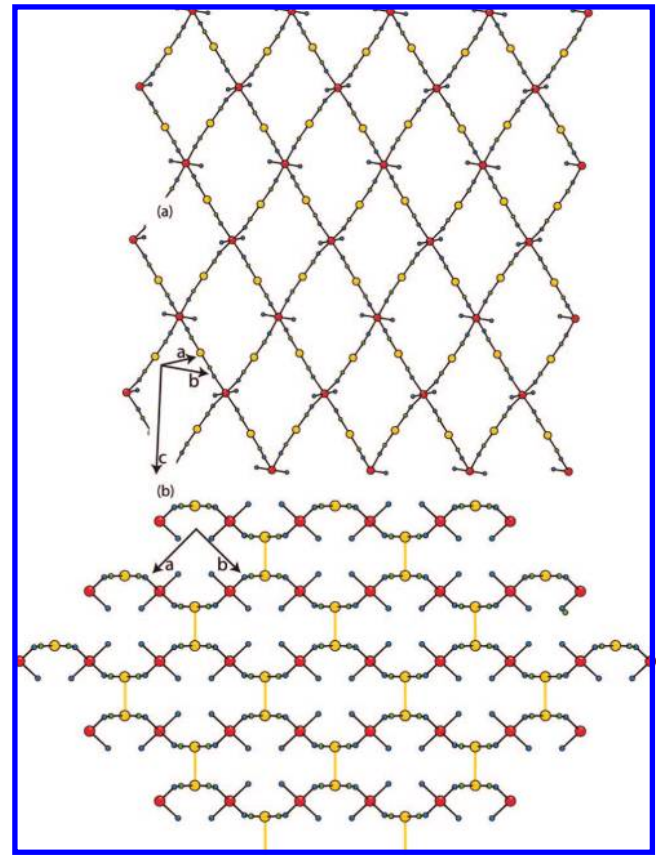


***Figure 11.*** Crystal structure of $\{Zn(NH_3)_2[Au(CN)_2]_2\}$: (a) corrugated sheet; (b) side view of stacked sheets.

to those in ***γ*** are found. A second set of sheets are inclined with respect to and interpenetrate through the aforementioned parallel sheets.[68] These inclined, interpenetrating sheets show no close gold−gold bonds or other interactions to one another. The room-temperature photoluminescence spectrum of $\{Zn(NH_3)_2[Au(CN)_2]_2\}$ shows a single emission band at 500 nm with an excitation band at 400 nm (Figure 8), matching the Au−Au-distance/emission-energy correlation graph (Figure S3 in the Supporting Information).

TGA of $\{Zn(NH_3)_2[Au(CN)_2]_2\}$ showed a decrease in mass starting at room temperature and ending at 95 °C. This mass

loss is consistent with a loss of 2 equiv of ammonia (observed loss, 6%; calculated loss, 5.7%). As the temperature was increased, a second loss from 350 to 390 °C was observed, consistent with decomposition of the polymer via cyanide loss and formation of ZnO and Au (observed loss, 15.2%; calculated loss, 14.7%), as seen for **α**−***δ***. It should be noted that the ammonia loss also occurred without heating: when $\{Zn(NH_3)_2[Au(CN)_2]_2\}$ was left open to air for 30 min, all of the ammonia molecules were released, leaving behind a white powder of $Zn[Au(CN)_2]_2$. Interestingly, the X-ray powder diffractogram of this ammonia-free product indicated that a mixture of the **α** and ***δ*** polymorphs had been generated. However, the ratio of the two polymorphs was sample-dependent; pure **α**, pure ***δ***, and various **α**/***δ*** ratios in between were all observed, and the factor(s) controlling the **α**/***δ*** ratio remains unclear. Photoluminescence spectra of the mixtures were consistent with the luminescence of **α** and mixtures of **α** and nonemissive ***δ***. It is important to note that reintroduction of ammonia vapor to any mixture of **α** and ***δ*** or even to pure ***δ*** invariably regenerated the saturated $[Zn(NH_3)_4][Au(CN)_2]_2$ complex followed by the bis(ammonia) complex $\{Zn(NH_3)_2[Au(CN)_2]_2\}$ (as confirmed by powder X-ray diffraction measurements in situ) upon removal of the ammonia-rich atmosphere.

In order to probe the mechanism of adsorption/desorption,[101] each of the four polymorphs was titrated with sequential equivalents of $NH_3$ while the $\nu_{CN}$ stretch in the IR spectrum was monitored. Titrations of **α** and ***δ*** revealed that they bind ammonia in a stepwise fashion (eq 5), first yielding $\{Zn(NH_3)_2[Au(CN)_2]_2\}$ ($\nu_{CN}$ = 2158 cm $^{-1}$) and then $[Zn(NH_3)_4][Au(CN)_2]_2$ ($\nu_{CN}$ = 2141 cm $^{-1}$):

$$(\alpha/\delta)Zn[Au(CN)_2]_2 + 2NH_{3(g)} \rightarrow \{Zn(NH_3)_2[Au(CN)_2]_2\}$$
$$\{Zn(NH_3)_2[Au(CN)_2]_2\} + 2NH_{3(g)} \rightarrow [Zn(NH_3)_4][Au(CN)_2]_2 \quad (5)$$

This reaction is completely reversible: loss of ammonia regenerates the same polymorph. However, titrations of ***β*** and ***γ*** revealed that the tetraamminezinc(II) complex forms directly (eq 6), with no $\{Zn(NH_3)_2[Au(CN)_2]_2\}$ intermediate being observed:

$$(\beta/\gamma)Zn[Au(CN)_2]_2 + 4NH_{3(g)} \rightarrow \{Zn(NH_3)_4[Au(CN)_2]_2\}$$
$$[Zn(NH_3)_4][Au(CN)_2]_2 \rightarrow \{Zn(NH_3)_2[Au(CN)_2]_2\} + 2NH_3(g) \quad (6)$$

Apparently, sufficient ammonia must be present to break all of the bonds between Zn(II) and the four cyanides in order for the initial $NH_3$ uptake to occur. Because of the adsorption routes for the four polymorphs, it is clear that once $[Zn(NH_3)_4][Au(CN)_2]_2$ is formed from ***β*** and ***γ***, these polymorphs cannot be regenerated upon $NH_3$ desorption; mixtures of **α** and ***δ*** are produced instead.

Porosity measurements on all four polymorphs showed no adsorption of nitrogen gas at 77 K. Therefore, **α**−***δ*** are not porous. Despite this, **α**−***δ*** reversibly bind ammonia vapor. It is well-known that nonporous coordination polymers can be quite flexible in the solid state.[102–104] The $d^{10}$ Zn(II) cation can adopt several geometries encompassing coordination numbers from 2 to 6;[49,98,105] undoubtedly, this flexibility facilitates the structural rearrangement which occurs as the ammonia interacts with the Zn(II) center. It should be noted that although binding of $NH_3$ occurs at Zn(II), it is the array of $Au(CN)_2^-$ units that act as the sensor, as the structural rearrangement changes the gold−gold distance and thus the emission energy.

Ammonia sensors are used in a wide range of settings.[93] The ideal sensor for each application has different requirements, including detection limits (0.1 ppb to 200 ppm), response times (seconds to minutes), and operating temperatures (0 to 500 °C).[93] Because of the great variation in these requirements, several different types of sensors are employed in the detection of ammonia. Some common ammonia-sensor materials include conducting compounds based on metal oxides[106–108] or polymers such as polypyrrole[109] and polyaniline;[110] other sensors are based on spectrophotometric determination.[111,112] While metal oxide-based sensors are very common, they require high operating temperatures, making them unsuitable in some applications, such as medical diagnostics.[93] Conversely, although atomic-absorption-based sensing can be operated at room temperature with high sensitivity, it is extremely expensive.[93]

This work clearly shows that all four polymorphs **α**−***δ*** act as vapoluminescent sensors for ammonia. In order to determine whether these $Zn[Au(CN)_2]_2$ materials (which are relatively inexpensive and quite stable) can compete with current $NH_3$ detection systems, quantitative detection limits for each polymorph were measured by monitoring the intensity of the $\{Zn(NH_3)_2[Au(CN)_2]_2\}$ emission band ($\lambda_{max}$ = 500 nm, $\lambda_{ex}$ = 400 nm) at 520 nm. Although the sensitivities of the polymers varied depending on polymorph, the lowest $NH_3$ detection limit (1 ppb) was observed for ***β***. The response times were also fast, on the order of seconds for all of the polymorphs. In comparison with other materials used as ammonia sensors, these four coordination polymers have some of the lowest $NH_3$ detection limits and fastest response times.

## Conclusion

The reactions of various zinc salts with the linear, anionic bridging ligand $Au(CN)_2^-$ formed four structurally unique polymorphs, three of which are luminescent at room temperature. Care had to be taken when synthesizing these polymorphs, since changing the concentration, counterion, pH, and/or solvent could redirect the synthesis from one polymorphic form to another. All four polymorphs reversibly act as very sensitive sensors for ammonia vapor, changing their emission energies

(101) Reller, A.; Oswald, H.-R. *J. Therm. Anal.* **1994**, *41*, 535.
(102) Kaneko, W.; Ohba, M.; Kitagawa, S. *J. Am. Chem. Soc.* **2007**, *129*, 13706.
(103) Kitagawa, S.; Kitaura, R.; Noro, S.-I. *Angew. Chem., Int. Ed.* **2004**, *43*, 2334.
(104) Batten, S. R.; Murray, K. S. *Aust. J. Chem.* **2001**, *54*, 605.
(105) Cole, S. C.; Coles, M. P.; Coles, P. B. *Dalton Trans.* **2003**, 3663.
(106) Rout, C. S.; Hegde, M.; Govindaraj, A.; Rao, C. N. R. *Nanotechnology* **2007**, *18*, 205504.
(107) Galbarra, D.; Arregui, F. J.; Matias, I. R.; Claus, R. O. *Smart Mater. Struct.* **2005**, *14*, 739.
(108) Thangadurai, V.; Weppner, W. *Solid State Ionics* **2004**, *174*, 175.
(109) Vidotti, M.; Dall'Antonia, L. H.; Cintra, E. P.; Córdobade Torresi, S. I. *Electrochim. Acta* **2004**, *49*, 3665.
(110) Lee, Y.-S.; Song, K.-D.; Huh, J.-S.; Chung, W.-Y.; Lee, D.-D. *Sens. Actuators, B* **2005**, *108*, 292.
(111) Yagi, T.; Kuboki, N.; Suzuki, Y.; Uchino, N.; Nakamura, K.; Yoshida, K. *Opt. Rev.* **1997**, *4*, 596.
(112) Malins, C.; Doyle, A.; MacCraith, B. D.; Kvasnik, F.; Landl, M; Šimon, P.; Kalvoda, L.; Lukaš, R.; Pufler, K.; Babusík, I. *J. Environ. Monit.* **1999**, *1*, 417.

as ammonia is bound. The emission can be correlated to the gold−gold array distance in each compound. The abilities of the polymorphs to selectively sense other gases and volatile organic compounds are currently under investigation.

**Acknowledgment.** The authors thank NSERC of Canada and the Natural Resources Canada Internship program (M.J.K.) for financial support and Professor Ken Sakai and Mr. Yuma Kuroki (Kyushu University, Japan) for the measurement of the emission lifetime of **α**.

**Supporting Information Available:** Single-crystal X-ray crystallographic data for ***β*** and ***δ*** in CIF format, powder X-ray data and fractional atomic coordinates for ***γ*** and $\{Zn(NH_3)_2[Au(CN)_2]_2\}$, and a plot of emission energy versus gold−gold distance. This material is available free of charge via the Internet at http://pubs.acs.org.

JA801773P